Surface Chemistry

DOI: 10.1002/ange.201207857

Ultralow Voltage Electrowetting on a Solidlike Ionic-Liquid Dielectric Layer**

*Xiaoning Zhang and Yuguang Cai**

Electrowetting has been widely used in devices like e-ink displays, digital microfluidics, liquid lens, and microelectricity generators, in which a 50–200 V driving voltage is used.[1–6] A lower driving voltage would offer better device stability. Here, we demonstrate electrowetting effects on an ionic-liquid (IL) dielectric layer using driving voltage of just 70 mV and 5 V in alternating and direct current (AC and DC) mode, respectively. Our data suggest that the ultrahigh capacitance of the IL dielectric layer directly leads to the low-voltage electrowetting.

The electrowetting can be described by the Lippmann Equation (1),

$$\gamma_{SL} = \gamma_{SL}^{0} - \frac{1}{2}CV^2 \quad (1)$$

where γ_{SL}^{0} is the voltage-free solid–liquid interface energy, C is the capacitance between the drop and surface, V is the applied voltage.[7,8] In the case of electrowetting on dielectrics (EWOD), the capacitance C can be expressed by Equation (2),

$$C = \frac{\varepsilon_0 \varepsilon_r A}{d} \quad (2)$$

where ε_0 is the permittivity in vacuum, ε_r is the dielectric constant, A is the contact area of the drop and d is the thickness of the dielectric layer. The contact angle can be expressed according to the Young Equation (3).

$$\cos\theta = \frac{\gamma_S - \gamma_{SL}}{\gamma_L}, \quad (3)$$

Combining Equations (1)–(3), we get Equation (4).

$$\theta = \arccos\left(\frac{\gamma_S - \gamma_{SL}^{0} + \frac{\varepsilon_0 \varepsilon_r A}{2d} V^2}{\gamma_L}\right). \quad (4)$$

Equation (4) suggests that there are two parallel approaches to reduce the driving voltage. One way is to increase the capacitance, either by decreasing the dielectric layer thickness or employing a coating with high dielectric constant; the other way is to minimize the interfacial energies of the solid $(\gamma_S - \gamma_{SL}^{0})$ and the liquid (γ_L), usually through using an immiscible oil bath.[6,9] The first approach can reduce the driving voltage down to about 15 V by employing a thin fluoropolymer coating.[10,11] If combined with the oil bath approach, electrowetting can be achieved at less than 3 V, at the price of incompatibility with digital microfluidic applications.[12]

We found that on a solidlike IL adsorbate layer, oil bath-free electrowetting could be achieved at an ultralow driving voltage. The IL layer acted as an electric double layer (EDL) with a high stability and ultrahigh capacitance density.[13,14] As a functional dielectric layer the IL-EDL leads to ultralow voltage electrowetting according to Equation (4).

Figure 1 shows the experimental setup and representative images of a 1-butyl-3-methylimidazolium chloride ([Bmim]Cl) drop on an octadecyltrichlorosilane (OTS) film at 0 V (Figure 1b) or −5 V (Figure 1c). The top views of the drop (Figure 1b/c) indicate that the contact line of the drop advanced after application of the voltage. Since [Bmim]Cl did not evaporat and thus the drop volume did not change, the contact line advancement corresponded to the decrease of the contact angle, demonstrating the electrowetting effect at

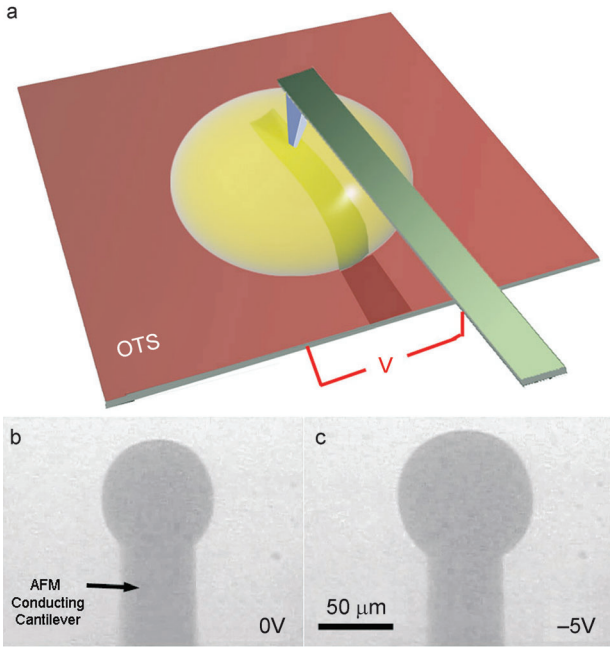

Figure 1. The electrowetting experiment. a) Scheme of the setup. b) Top view of the [Bmim]Cl drop on an OTS surface with no voltage applied. c) The same drop with −5 V applied. The experiment was conducted in a N_2 environment. The drop volume is 100 pL.

[*] X. N. Zhang, Prof. Y. G. Cai
Department of Chemistry, University of Kentucky
505 Rose Street, Lexington, KY (USA)
E-mail: ycai3@uky.edu

[**] This research is partially supported by the University of Kentucky faculty start-up fund. X. Zhang thanks the support from the Chinese Government Scholarship and the Kentucky Opportunity Fellowship.

Supporting information for this article is available on the WWW under http://dx.doi.org/10.1002/anie.201207857.

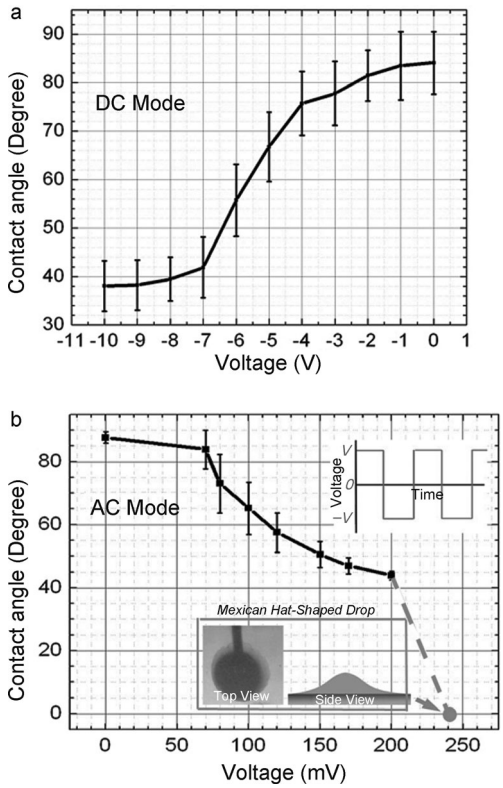

Figure 2. The contact angle of a [Bmim]Cl drop on the OTS surface as a function of the applied voltage in a) DC and b) AC modes. The 400 Hz AC bias is shown in the upper inset. When the voltage $V > 240$ mV, the drop changed from the spherical cap shape to the Mexican hat shape. The lower inset shows the top-view photograph and side-view model of the Mexican hat-shaped drop. The dashed plot indicates that the contact angle is the apparent contact angle near the edge of the Mexican hat-shaped drop.

−5 V. Figure 2 shows the contact angle as a function of the voltage for [Bmim]Cl drops on an OTS film in DC and AC modes. In the DC mode, electrowetting started at −4 V and the contact angle decreased a total of 42 degrees at −7 V. As a reference, on a fluoropolymer surface the contact angle of a [Bmim]Cl drop decreases only a total of 18 degrees at 50 V in DC mode.[15]

We found that the AC bias can generate electrowetting at lower voltage, which is similar to the earlier result from the Armstrong group.[16] Figure 2b shows that the electrowetting in AC mode started at 70 mV. When the voltage was higher than 240 mV, a thin liquid layer surrounding the drop appeared and slowly spread out. During the spreading, the drop adopted a Mexican hat shape, as shown in the inset in Figure 2b. The apparent "contact angle" near the edge of the "Mexican hat" (the rim) was close to 0°. Electrowetting in AC mode occurred at < 240 mV and also indicates that the observed contact angle change is not associated with any potential electrochemical reaction since all chemicals involved in the experiment (IL, OTS, and Si) are stable at 240 mV bias.

We also tested the electrowetting of two additional representative ILs (1-butyl-3-methylimidazolium bis(trifluoromethylsulfonyl) imide ([Bmim][Tf_2N]) and 1-decyl-3-methylimidazolium chloride ([C_{10}mim]Cl) on the OTS surface. Both ILs showed low-voltage electrowetting at driving voltages < 10 V. Figure 3a&b shows the electrowetting of [Bmim][Tf_2N] on the OTS film driven by a 10 V DC bias. The contact angle (CA) dropped from 63° to 50°. The full AC and DC mode electrowetting process of [Bmim][Tf_2N] can be seen in the video clips in the Supporting Information (sections 1 and 2). In Figure 3c the CA is plotted during the AC mode electrowetting, indicating that the electrowetting for [Bmim][Tf_2N] on OTS is a reversible process. The electrowetting of [Bmim][Tf_2N] was employed as RC filter.[17] Our results show that the filter setup can be simplified by omitting the Teflon coating on the substrate, which would offer an improved low-voltage filtering performance.

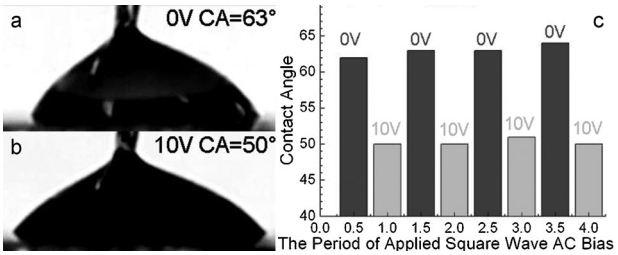

Figure 3. Side views of a [Bmim][Tf_2N] drop on an OTS surface a) without bias and b) at 10 V. c) The contact angle of the same drop driven by a 1 Hz AC mode square wave bias during four periods. The contact angles are obtained from a video clip in Supporting Information (section 2).

After the electrowetting experiment, we used a stream of nitrogen to blast the [Bmim]Cl drop off the surface as illustrated in Figure 4a/b. Figure 4c,d displays AFM images of the surface (blue box in Figure 4b) after the blast. The left side of Figure 4c,d was the OTS surface, which was outside of the drop and never in contact with the IL; whereas the right part was previously covered by the IL drop. Figure 4c (topography) shows that the IL adsorbate layer was higher than the OTS surface. The height histogram of the topography (inset in Figure 4d) reveals that the IL adsorbate layer was 6.4 Å higher than the OTS surface. In addition, the phase image (Figure 4d) reveals that the IL adsorbate layer had a higher phase signal than the OTS surface, indicating that the tip dissipated more energy tapping over this surface than over the OTS surface.

These observed differences in both the topographies and phase channels reveal that the right part of the surface is a [Bmim]Cl layer adsorbed on OTS. Furthermore, this adsorbed layer formed at the liquid [Bmim]Cl–OTS interface when the IL drop sat on the OTS surface. In the topography image, additional "green" dropletlike features were visible. The left height scale indicates that these green features were on top of the [Bmim]Cl adsorbate layer and were 5–8 nm higher than the layer. In the corresponding phase image, these green features had significantly higher phase signals than the [Bmim]Cl adsorbate layer. When we slightly decreased the tapping amplitude set point, that is, tap the surface harder, oscillations occurred over these green features. Such behavior is characteristic of a liquid. Oscillations indicated that the tip

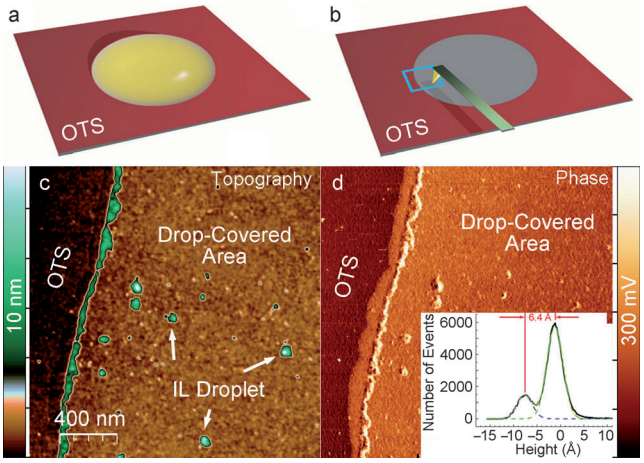

Figure 4. AFM image of the drop edge after the drop was blasted off the surface. a) Schematic view of a [Bmim]Cl drop sitting on the OTS surface. b) The drop was removed. AFM was used to characterize the area (within the blue box) over the drop edge. c) The topography channel of the AFM image. The green features are the liquid phase [Bmim]Cl remaining on the surface. The green line is the position of the drop edge. On the left side of the edge is a clean OTS surface, which was not covered by the drop. The right side of the edge is the surface previously covered by the IL drop. d) The phase image. The green features in the topography appear as white spots in the phase channel, indicating that the tip dissipated a huge energy tapping over them. The topography histogram (inset in d) indicates that the surface under the drop is 6.4 Å higher than the clean OTS surface.

tapped into liquid and induced perturbations. Therefore, these green features were remaining droplets of the liquid phase of [Bmim]Cl on the [Bmim]Cl adsorbate layer. Furthermore, since the phase image (Figure 4 d) reveals that the [Bmim]Cl adsorbate layer and the [Bmim]Cl droplet have different contrasts, they are in different phases. The liquid phase [Bmim]Cl droplet did not wet or dissolve the [Bmim]Cl adsorbate layer.

In a separated test, we applied a 10 V and −10 V bias to two spots in the IL layer using a conductive AFM tip, respectively. Then we imaged the layer again with AFM in AC mode. We did not observe any change in height or surface properties for the two spots in the layer. Thus, the solidlike IL layer was stable in the electric field.

Figure 5 shows the suggested interface structure based on our AFM characterization. A solidlike [Bmim]Cl layer formed at the liquid–OTS interface. The liquid [Bmim]Cl drop sat on top of the [Bmim]Cl layer. In a control experiment, we applied a 10 V bias voltage between a conducting AFM tip and a clean OTS-coated silicon wafer. Subsequent AFM characterization revealed that the OTS film was partially degraded and formed a carboxylic-terminated chemical pattern. In this oxidation process, current was detected, indicating that both the native oxide and the OTS film were not a dielectric layer. Rather, the OTS-coated silicon substrate was the electrode in the EWOD system. Therefore, the functioning dielectric layer was the solidlike IL adsorbate layer at the liquid–OTS interface.

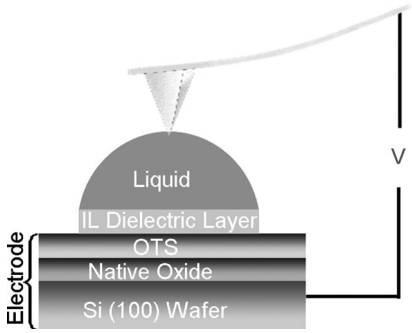

Figure 5. The structure of the low-voltage electrowetting system.

ILs have been known to form layers at the liquid–solid interface when the IL contacts either a charged surface or a neutral surface.[19–26] The first layer at the interface is tightly packed and solidlike, whereas other IL layers gradually change into disordered liquid phases. Figure 4 revealed that upon contacting OTS, [Bmim]Cl formed a solidlike adsorbate layer, which is consistent with published results on other ILs.[19–26] The IL interface layer has a very high charge carrier density and an ultrahigh capacitance density at the level of 0.01–0.1 $F\,m^{-2}$.[14,26,27] Hence the observed solidlike IL adsorbate layer was a functional dielectric layer with an ultrahigh capacitance density in the EWOD system. We suggest that the ultrahigh capacitance of the IL dielectric layer is the reason for the observed low-voltage electrowetting.

As indicated in Equation (4), once the voltage is applied, the contact angle decreases, which corresponds to the advancement of the contact line. Liquid-phase ILs would cover a fresh OTS surface. With the help of an electric field within the drop, the IL dielectric layer will form immediately on the new OTS–IL interface covered by the drop. If the IL dielectric layer had not formed at the fresh OTS–liquid phase IL interface, according to Figure 5, the conductive IL would connect the two electrodes (the wire in the drop and the OTS, which served as an electrode, as indicated in the previous control experiment). Electrostatic charges on the drop surface would not exist. As a result, electrowetting would not occur and we should observe that the contact line of the drop retracted. Since this scenario did not happen, we conclude that the IL dielectric layer buried at the liquid–solid interface formed immediately after the IL contacted the OTS surface.

Previous studies on the electrowetting of ILs on the dielectric layer of a fluoropolymer have shown that the electrowetting started from >15 V.[15,16,28] Since ILs can form a dielectric layer at the liquid–solid interface, employing an additional fluoropolymer coating would put the capacitance of the IL dielectric layer (C_{IL}) and the capacitance of the dielectric layer of the fluoropolymer (C_f) in series. Thus the overall capacitance C_{total} could be expressed as Equation (5).

$$\frac{1}{C_{total}} = \frac{1}{C_{IL}} + \frac{1}{C_f} \tag{5}$$

If C_{IL} is much larger than C_f, C_{total} would be similar to C_f. Hence the effect of the IL dielectric layer would not be observed. Our study reveals that the fluoropolymer coating for IL electrowetting is unnecessary. The solidlike IL layer can directly serve as the dielectric layer.

Defects in the dielectric layer are responsible for the failure of EWOD devices because small ions can diffuse into these defects.[18] The IL–OTS electrowetting system (IL on a solidlike IL dielectric layer, ILOSILD) could avoid such dielectric layer break-down because the liquid-phase IL on top of the dielectric layer could automatically replenish the defects and hot spots inside the dielectric layer, restoring the integrity of the dielectric layer. In the mean time, the bulky size of the ions in the IL also suppresses diffusion.

The IL dielectric layer could also support the low-voltage electrowetting of other liquids, providing that the drop did not dissolve the layer. In the Supporting Information (section 5), we show the low-voltage electrowetting of a water drop on a [Bmim][Tf_2N] dielectric layer, which started from −1 V. We also saw low-voltage electrowetting of other aqueous salt, protein, and DNA solutions on the [Bmim][Tf_2N] dielectric layer.

In summary, we reported a new approach for oil-bath-free low-voltage electrowetting. Drops on a IL-coated surface showed electrowetting at driving voltages as low as 70 mV. AFM revealed that the IL formed a solidlike adsorbate film, which was immiscible with liquids and served as a dielectric layer in the EWOD system. The ultrahigh capacitance density of the IL dielectric layer led to low-voltage electrowetting.

Our ultralow voltage electrowetting approach could simplify the digital microfluidic design, and enable new studies on liquid lenses and e-ink displays because liquid drops on the surface can be manipulated by the electrowetting effect without an oil bath. Furthermore, since the driving voltage could be lower than 5 V, most electrowetting experiments can be directly driven by digital integrated circuit chips, or computer output ports without voltage escalation circuitry. Therefore, the high technical barrier to study and develop electrowetting applications would be drastically reduced.

Experimental Section

The surface used for electrowetting was an OTS-coated silicon wafer. The silicon (100) wafers (cleaned by a piranha solution, ultraflat with a root-mean-square roughness < 5 Å) were incubated in a 5 mM OTS toluene solution at 20 °C overnight to form an OTS monolayer silane coating. The OTS film (26 Å thick) has defects. Water, ions, small organic silane molecules can fill into defect sites. OTS was not an insulating layer. OTS served as a hydrophobic coating on the electrode. [Bmim]Cl was incubated in a vacuum oven at 80 °C overnight to remove the water in the IL before the experiment.

Figure 1 a shows the electrowetting setup. The wafer was mounted on an AFM sample holder and grounded. The bias voltage was applied through a conducting AFM probe. The drop was viewed through the top video camera on the microscope. For the electrowetting test of the water drop, the relative humidity (RH) inside environmental chamber was maintained at 100 % to prevent drop evaporation during the experiment.

The contact angle of the drop was calculated from the diameter and the height of the drop. The methodology is explained in the Supporting Information (section 4). The side-view contact angle was obtained using Image J and contact angle analysis plug-in.[29]

Received: September 28, 2012
Revised: December 18, 2012
Published online: January 16, 2013

Keywords: atomic force microscopy · dielectric layers · electrowetting · ionic liquids · surface chemistry

[1] F. Mugele, J. C. Baret, *J. Phys. Condens. Matter* **2005**, *17*, R705.
[2] T. Krupenkin, J. A. Taylor, *Nat. Commun.* **2011**, *2*, 448.
[3] H. You, A. J. Steckl, *Appl. Phys. Lett.* **2010**, *97*, 023514.
[4] R. B. Fair, *Microfluid. Nanofluid.* **2007**, *3*, 245.
[5] B. Berge, J. Peseux, *Eur. Phys. J. E* **2000**, *3*, 159.
[6] S. Chevalliot, J. Heikenfeld, L. Clapp, A. Milarcik, S. Vilner, *J. Disp. Technol.* **2011**, *7*, 649.
[7] B. Shapiro, H. Moon, R. L. Garrell, C. J. Kim, *J. Appl. Phys.* **2003**, *93*, 5794.
[8] A. Quinn, R. Sedev, J. Ralston, *J. Phys. Chem. B* **2005**, *109*, 6268.
[9] S. G. Zhang, X. D. Hu, C. Qu, Q. H. Zhang, X. Y. Ma, L. J. Lu, X. L. Li, X. P. Zhang, Y. Q. Deng, *ChemPhysChem* **2010**, *11*, 2327.
[10] M. Vallet, M. Vallade, B. Berge, *Eur. Phys. J. B* **1999**, *11*, 583.
[11] H. Moon, S. K. Cho, R. L. Garrell, C. J. Kim, *J. Appl. Phys.* **2002**, *92*, 4080.
[12] S. Berry, J. Kedzierski, B. Abedian, *J. Colloid Interface Sci.* **2006**, *303*, 517.
[13] A. Quinn, R. Sedev, J. Ralston, *J. Phys. Chem. B* **2003**, *107*, 1163.
[14] J. T. Ye, S. Inoue, K. Kobayashi, Y. Kasahara, H. T. Yuan, H. Shimotani, Y. Iwasa, *Nat. Mater.* **2010**, *9*, 125.
[15] Y. S. Nanayakkara, H. Moon, T. Payagala, A. B. Wijeratne, J. A. Crank, P. S. Sharma, D. W. Armstrong, *Anal. Chem.* **2008**, *80*, 7690.
[16] Y. S. Nanayakkara, S. Perera, S. Bindiganavale, E. Wanigasekara, H. Moon, D. W. Armstrong, *Anal. Chem.* **2010**, *82*, 3146.
[17] Y. S. Nanayakkara, H. Moon, D. W. Armstrong, *ACS Appl. Mater. Interfaces* **2010**, *2*, 1785.
[18] B. Raj, M. Dhindsa, N. R. Smith, R. Laughlin, J. Heikenfeld, *Langmuir* **2009**, *25*, 12387.
[19] R. Atkin, G. G. Warr, *J. Phys. Chem. C* **2007**, *111*, 5162.
[20] S. Perkin, T. Albrecht, J. Klein, *Phys. Chem. Chem. Phys.* **2010**, *12*, 1243.
[21] L. Tamam, B. M. Ocko, H. Reichert, M. Deutsch, *Phys. Rev. Lett.* **2011**, *106*, 197801.
[22] Y. Yokota, T. Harada, K. I. Fukui, *Chem. Commun.* **2010**, *46*, 8627.
[23] S. Bovio, A. Podesta, C. Lenardi, P. Milani, *J. Phys. Chem. B* **2009**, *113*, 6600.
[24] C. Romero, S. Baldelli, *J. Phys. Chem. B* **2006**, *110*, 6213.
[25] S. A. Kislenko, I. S. Samoylov, R. H. Amirov, *Phys. Chem. Chem. Phys.* **2009**, *11*, 5584.
[26] J. Z. Wu, T. Jiang, D. E. Jiang, Z. H. Jin, D. Henderson, *Soft Matter* **2011**, *7*, 11222.
[27] H. T. Yuan, H. Shimotani, J. T. Ye, S. Yoon, H. Aliah, A. Tsukazaki, M. Kawasaki, Y. Iwasa, *J. Am. Chem. Soc.* **2010**, *132*, 18402.
[28] M. Paneru, C. Priest, R. Sedev, J. Ralston, *J. Am. Chem. Soc.* **2010**, *132*, 8301.
[29] A. F. Stalder, T. Melchior, M. Muller, D. Sage, T. Blu, M. Unser, *Colloids Surf. A* **2010**, *364*, 72.

